Salicylamide Cocrystals: Screening, Crystal Structure, Sublimation Thermodynamics, Dissolution, and Solid-State DFT Calculations

ARTICLE *in* THE JOURNAL OF PHYSICAL CHEMISTRY B · MAY 2014

Impact Factor: 3.3 · DOI: 10.1021/jp5032898 · Source: PubMed

7 AUTHORS, INCLUDING:

Alexey Manin
Institute of Solution Chemistry of RAS
22 PUBLICATIONS **100** CITATIONS
SEE PROFILE

N. G. Manin
Institute of Solution Chemistry of RAS
54 PUBLICATIONS **141** CITATIONS
SEE PROFILE

Mikhail V Vener
Mendeleev Russian University of Chemical Tec…
69 PUBLICATIONS **1,186** CITATIONS
SEE PROFILE

German L Perlovich
Institute of Solution Chemistry of RAS
142 PUBLICATIONS **1,475** CITATIONS
SEE PROFILE

THE JOURNAL OF PHYSICAL CHEMISTRY B

Article

pubs.acs.org/JPCB

Salicylamide Cocrystals: Screening, Crystal Structure, Sublimation Thermodynamics, Dissolution, and Solid-State DFT Calculations

Alex N. Manin,[†] Alexander P. Voronin,[†] Nikolay G. Manin,[†] Mikhail V. Vener,[‡] Anastasia V. Shishkina,[‡] Anatoly S. Lermontov,[§] and German L. Perlovich*,[†]

[†]G.A. Krestov Institute of Solution Chemistry of the Russian Academy of Sciences, 1, Academicheskaya, 153045 Ivanovo, Russia

[‡]Mendeleev University of Chemical Technology, 9, Miusskaya Square, 125047 Moscow, Russia

[§]Kurnakov's Institute of General and Inorganic Chemistry, Russian Academy of Sciences, 119991 Moscow, Russia

Supporting Information

ABSTRACT: A new cocrystal of 2-hydroxybenzamide (A) with 4-acetamidobenzoic acid (B) has been obtained by the DSC screening method. Thermophysical analysis of the aggregate [A:B] has been conducted and a fusion diagram has been plotted. Cocrystal formation from melts was studied by using thermomicroscopy. A cocrystal single-crystal was grown and its crystal structure was determined. The pattern of noncovalent interactions has been quantified using the solid-state DFT computations coupled with the Bader analysis of the periodic electron density. The sublimation processes of A-B cocrystal have been studied and its thermodynamic functions have been calculated. The classical method of substance transfer by inert gas-carrier was chosen to investigate sublimation processes experimentally. The lattice energy is found to be 143 ± 4 kJ/mol. It is lower than the sum of the corresponding values of the cocrystal pure components. The theoretical value of the lattice energy, 156 kJ/mol, is in reasonable agreement with the experimental one. A ternary phase diagram of solubility (A-B−ethanol) has been plotted and the areas with solutions for growing thermodynamically stable cocrystals have been determined.

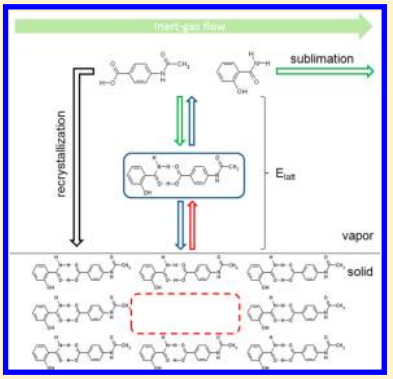

1. INTRODUCTION

Solubility is one of the significant parameters that have an impact on drug therapeutic effectiveness. At the present time, a new method for improving the solubility by obtaining two-component crystals has gained increased interest.[1] These species, known more commonly as pharmaceutical cocrystals, consist of an active pharmaceutical ingredient (API) and a second component that is a solid under ambient conditions, linked by intermolecular forces. The second component should be safe for human consumption and is often referred to as the cocrystal former (coformer). These cocrystals are a possible way to modify the physicochemical properties of the active pharmaceutical ingredients,[2−4] such as solubility,[5] physical[6] and mechanical[7] properties, thermodynamic stability,[8] etc., without changing the pharmacological activity.

The creation of pharmaceutical cocrystals is an area of expanding growth.[9−14] The key design tool used to select a suitable compound (a cocrystal former) for a given substance is the concept of supramolecular synthon.[15] Several types of supramolecular synthon are usually realized in two-component crystals and are characterized by intermolecular hydrogen bonds (H-bonds) of different types and strengths (see Scheme 1).[16] The energy of these interactions was evaluated in a number of papers.[17,18] It reaches 64 kJ/mol in the acid-amide heterosynthon. A lot less attention has been paid to the quantitative description of the intermolecular interactions of homo- and heterodimers with the neighbor molecules which play an important role in the successful cocrystal phase formation.[19] The cumulative characteristic of the intermolecular (noncovalent) interactions in solids is the sublimation enthalpy

Scheme 1. Representative supramolecular synthons. I and II, acid−acid and amide−amide homosynthons; III and IV, acid−amide and acid−pyridine heterosynthons

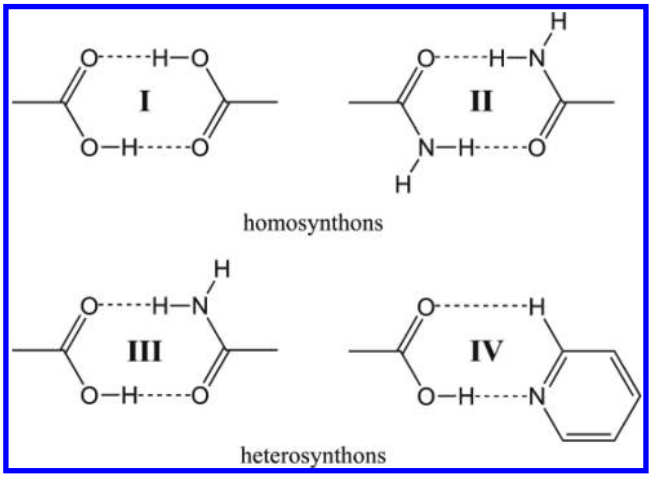

Received: April 3, 2014
Revised: May 23, 2014
Published: May 25, 2014

   dx.doi.org/10.1021/jp5032898 | J. Phys. Chem. B 2014, 118, 6803−6814

ΔH_{sub}. This value extrapolated to 0 K corresponds to the crystal lattice energy, E_{latt}. The $\Delta H_{sub}/E_{latt}$ values in the molecular crystals were evaluated experimentally[20] and theoretically.[21,22] The results of the experimental studies of ΔH_{sub} in cocrystals have not been published yet.

The present paper considers the cocrystal of 2-hydroxybenzamide (salicylamide, A) with 4-acetamidobenzoic acid (acetamidobenzoic acid, B). This cocrystal is chosen for the following reasons. (i) The acid−amide heterosynthon is a persistent H-bond motif in cocrystal structures.[23] (ii) Salicylamide is an active pharmaceutical ingredient while acetamidobenzoic acid is safe for human consumption. (iii) The crystal structures and thermodynamic functions of sublimation for both components have been published earlier.[24] Summing up all the above-said, the aims of the paper can be presented as follows. (1) To screen the cocrystals between salicylamide and acetamidobenzoic acid isomers. (2) To investigate the crystal structure(s) of the obtained salicylamide cocrystal(s) by using X-ray diffraction analysis. (3) To study the cocrystal(s) sublimation process(es) and determine the thermodynamic characteristics thereof. (4) To describe quantitatively the pattern of the intermolecular interactions in the salicylamide cocrystal in terms of the Bader analysis of the periodic electron density. To compute the cocrystal lattice energy and to compare it with the experimental one. (5) To investigate dissolution process(es) of the considered cocrystal(s).

2. EXPERIMENTAL METHODS

2.1. Materials. Salicylamide and 4-acetamidobenzoic acid were purchased from Sigma-Aldrich in the highest purity available. The purity of these chemicals was over 98%. The materials were used as received.

2.2. Cocrystal Preparation and Solid-Phase Identification. *2.2.1. Mechanochemical Experiments.* The cocrystal powder samples were obtained by neat and liquid-assisted grinding. A 1:1 molar ratio mixture of components was placed into the agate milling jar of the "Pulverisette 7" planetary micromill and a corresponding quantity (about 1 μL per 1 mg of the mixture) of ethanol was added. The mixture was mixed for 30 min at 600 rpm with ten 5 mm agate balls. Then the jar was left for 5−10 min at a room temperature for the solvent to evaporate. The purity of the cocrystals obtained was controlled by observing the quantity of endotherms at the DSC curve and PXRD experiment.

2.2.2. Crystallization from Solution. The single crystals used in X-ray experiments were obtained by crystallization from solution. A 1:1 molar ratio mixture of components was completely dissolved in a slightly exceeding volume of solvent (ethanol), filtered through PTFE filter (0.45 μm) and left at the room temperature until the solvent evaporated. Colorless crystalline plates suitable for single crystal X-ray diffraction emerged after 2 weeks.

2.3. X-ray Diffraction Experiments. *2.3.1. PXRD Measurements.* PXRD measurements were performed using Bruker D8 Advance diffractometer with CuKα1 radiation (λ = 1.5406 Å). Data were collected within the 2θ range of 5−30° with a step size 0.03°.

2.3.2. Single-Crystal X-ray Diffraction Measurements. Single-crystal X-ray diffraction measurements were made using a Nonius CAD-4 diffractometer with graphite-monochromated Mo Kα radiation (λ = 0.71069 Å). Intensity data were collected at 120 K by means of a ω-2θ scanning procedure. The crystal structures were solved using direct methods and refined by means of a full-matrix least-squares procedure. CAD-4[25] was applied for data collection, data reduction and cell refinement. SHELXS-97 and SHELXL-97 programs[26] were used to solve and to refine structures, respectively.

2.4. Differential Scanning Calorimetry (DSC). Thermal analysis was carried out using a DSC 204 F1 Phoenix differential scanning heat flux calorimeter (NETZSCH, Germany) with a high sensitivity m-sensor. The sample was heated at the rate of 10 K·min^{-1} in an Ar atmosphere and cooled with liquid N_2. The temperature calibration of the DSC was performed against six high-purity substances, cyclohexane (99.96%), mercury (99.99+%), biphenyl (99.5%), indium (99.999%), tin (99.999%), and bismuth (99.9995%). The accuracy of the weighing procedure was ±0.01 mg.

2.5. Solubility Study. The solubility experiments were performed using the isothermal saturation method. The exceeding quantity of the substance and a certain amount of solvent are placed into the test tubes of an air thermostat and stirred at the controlled temperature. The average saturation time for most substances under study was 20−24 h. The fluctuations in temperature inside the thermostat were ±0.02 °C. After the saturation the solution was centrifuged at the experimental temperature for about 5 min, the aliquot was diluted and its UV absorbance was measured by the VARIAN CARY 50 spectrophotometer in the range of λ from 220 to 400 nm. All the equipment that was in contact with the saturated solution was thermostated at the experimental temperature. For each substance the experiment was performed three times. The maximal error of spectrophotometric experiments was 2−2.5%.

2.6. Hot Stage Microscopy (HSM). The thermal microscopy analysis was carried out using the Altami POLAR 312 polarization microscope equipped with a Microstate N-350 hot stage, an Altami USB 3150R6 1/2CMOS camera and an Altami Studio software package. The fine crystalline sample was placed between two laboratory glasses into the heating plate cell that was set under the objective lens of the microscope and was heated at various speeds until its transition to liquid state. The changes in crystal morphology and phase transitions in the sample were detected visually and using the USB-camera through the PL L 10X/0.25 plan achromatic lens. After melting, the morphology of the crystals obtained was compared to the morphology of one of the initial compounds.

2.7. Sublimation Measurements. Sublimation experiments were carried out by the transpiration method as was described elsewhere.[24,27] In brief: a stream of an inert gas passes above the sample at a constant temperature and at a known slow constant flow rate in order to achieve saturation of the carrier gas with the vapor of the substance under investigation. The vapor is condensed at some point downstream, and the mass of sublimate and its purity are determined by UV−vis spectrophotometry and DSC. The vapor pressure over the sample at this temperature can be calculated by the amount of the sublimated sample and the volume of the inert gas used. The sublimation experiment details are given in the Supporting Information.

2.8. DSC/TG/Mass-Spectrometry Experiment. Cocrystal sublimation thermodynamics experiments were carried out using a NETZSCH STA 409 CD/7/G + Skimmer DSC/DTA/TG with a Skimmer mass-spectrometric vapor analysis system (E_{ion} = 70 eV) in the argon flow at the rate of 70 mL/min. The powder sample was placed into a platinum crucible and heated

dx.doi.org/10.1021/jp5032898 | J. Phys. Chem. B 2014, 118, 6803−6814

at the rate of 10 K/min. The temperature was measured with a Pt10%−Pt−Rh thermocouple. The temperature calibration of the equipment was performed against eight high-purity substances: biphenyl (99.5%), κNO_3 (99.999%), $RbNO_3$ (99.99%), $KClO_4$ (≥99%), Ag_2SO_4 (99.999%), CsCl (99.999%), K_2CrO_4 (≥99%), and $BaCO_3$ (99.98%).

3. LATTICE ENERGY EVALUATION

There are several theoretical approaches to assessment of lattice energy in crystalline materials. The first one is based on phenomenological models (see paper of Kuleshova[12] for examples). A considerable potency of this approach for in silico screening of cocrystals, as well as their relative solubility has been demonstrated. However, this approach is based on simple thermodynamic arguments the physical meaning of which is vague.

In the second approach E_{latt} is evaluated using the total energy of the unit cell, E(bulk), and relaxed energies of the A and B molecules, E(A) and E(B), forming a supramolecular synthon:

$$E_{latt} = E(\text{bulk})/Z - E(\text{A}) - E(\text{B}) \quad (1)$$

Z is the number of supramolecular synthons in the cell. Equation 1 is exact for two-component crystals with $Z' = 1$. If the localized basis set is used in solid-state computations, the basis set superposition error (BSSE) has to be evaluated. This can be done using the MOLEBSSE option of the Crystal09 package.[28] Its applicability to the BSSE evaluation in cocrystals is not straightforward.[29]

The third approach views the lattice energy as a sum of the energies of noncovalent interactions between the considered molecule and its neighbors:[30]

$$E_{latt} = \sum_{j} \sum_{j<i} E_{int,j,i} \quad (2)$$

$E_{int,j,i}$ is the energy of the particular noncovalent (intermolecular) interaction; j and i denote the atoms belonging to different molecules. Equation 2 is the BSSE free. For the sake of simplicity, indexes j and i will be omitted below.

E_{int} may be evaluated using the pairwise potentials[31] or empirical formulas/approaches linking different properties of noncovalent interactions in crystals with their energy/enthalpy (see ref 32 for examples). To our best knowledge, eq 2 was used only in one paper[19] to assess the lattice energy of the salicylic acid-benzamide cocrystal and a series of model benzoic acid/benzamide cocrystals.

Details of the DFT computations with periodic boundary conditions (solid-state DFT calculations) are given in the Supporting Information. The optimized geometrical parameters of the cocrystal were used in the B3LYP/6-31G** computation of the periodic electronic wave functions by CRYSTAL98.[33] The quantum theory of atoms in molecules and crystals (QTAIMC) analysis[34] of the periodic electron density obtained from the crystalline wave function is performed with TOPOND.[35] The calculation methodology is presented elsewhere.[36] The following electron-density features at the bond critical point are computed: (i) the values of the electron density, ρ_b, (ii) the Laplacian of the electron density, $\nabla^2\rho_b$, and (iii) the positively defined local electronic kinetic energy density, G_b. Within the QTAIMC, the particular noncovalent intermolecular interaction is associated with the existence of the bond path (i.e., the bond critical point) between the pair of atoms. The absence of the bond critical point implies that the two atoms do not interact. The network of the bond paths yields the comprehensive bond picture, the energy of each specific interaction (in our case it is the intermolecular H-bond, C−H···O contact etc.) is considered totally independent of the others. The effects of crystal environment, long-term electrostatic effects etc. are taken into account implicitly, via the periodic electronic wave function, and are coded in the bond critical point features. The energy of the particular noncovalent interaction, E_{int}, is evaluated according to[37] as

$$E_{int} = 0.429G_b(\text{in atomic units}) \quad (3)$$

Equation 3 yields reasonable E_{int} values for molecular crystals with H-bonds, C−H···O and π-stacking contacts etc.[32,38]

4. RESULTS AND DISSCUSION

4.1. Cocrystal Screening and Thermal Analysis. For the binary systems of salicylamide with *i*-acetamidobenzoic acids, the probability of cocrystal formation was determined using the DSC cocrystal screening technique developed by Lu et al.[39] The experiments have shown that only one system, salicylamide (A): 4-acetamidobenzoic acid (B), has two endothermic peaks at a DSC curve of a 1:1 physical mixture (Figure 1) and, thus, is

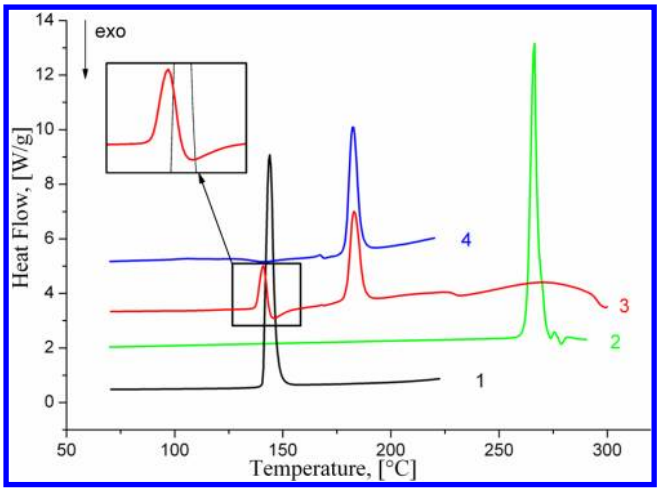

Figure 1. DSC curves of salicylamide (A) (1), 4-acetamidobenzoic acid (B) (2), A:B (1:1) physical mixture (3), and A:B (1:1) after solvent-drop grinding (4).

the only one capable of forming cocrystals. Moreover, the exothermic peak at 145.9 °C also corresponds to cocrystal formation as similar effects were observed by Yamashita et al.[40] in cocrystal-forming mixtures. For the other two systems, none of these criteria are met.

For every system, an experiment was made to obtain a pure cocrystal by neat cogrinding, as well as cogrinding in the presence of ethanol. It was found that the solvent-drop grinding of the A:B (1:1) with ethanol leads to only one phase transition at 182.4 °C on the DSC curve, which differs from both components' melting points and can be interpreted as the melting point of the pure 1:1 cocrystal ((4) in Figure 1).

To prove the DSC results, the fusion processes were visualized by hot stage microscopy (HSM). It was proved that the 1:1 mixtures of salicylamide with 2- and 3-acetamidobenzoic acid show a simple eutectic fusion. The HSM results for the salicylamide:4-acetamidobenzoic acid system are discussed in detail below.

dx.doi.org/10.1021/jp5032898 | J. Phys. Chem. B 2014, 118, 6803−6814

Several attempts were also made to obtain a cocrystal from acetone, methanol, and ethanol solutions through solvent evaporation. The DSC analysis of dried precipitates indicated the cocrystal formation in A:B with ethanol as solvent, while in other cases components crystallized separately.

To interpret the processes occurring while the physical mixture was heated, a fusion diagram was constructed based on a series of DSC experiments for A:B mixtures with different component ratios. This diagram presented in Figure 2 shows

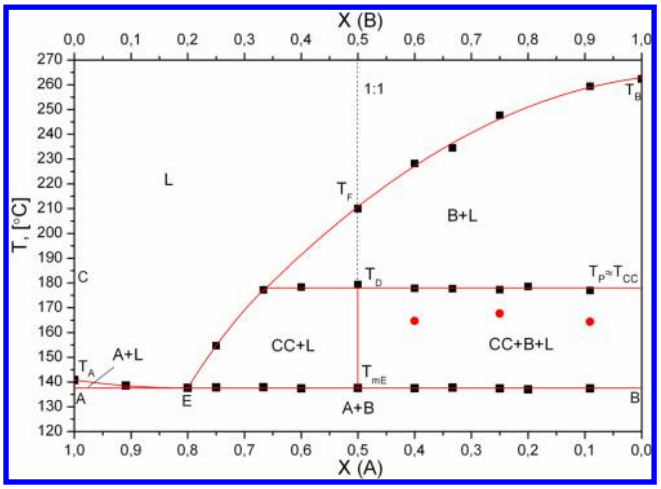

Figure 2. Fusion diagram of A:B physical mixture. L corresponds to liquid; A, salicylamide; B, 4-acetamidobenzoic acid; CC, cocrystal; E, eutectic point; T_P, peritectic temperature; T_A, melting temperature of A; T_B, melting temperature of B; T_{CC}, melting point of cocrystal; T_{mE}, metastable eutectic temperature. Description of the red circles sees in the text.

that the system we deal with melts incongruently. When the 1:1 mixture is heated at T_{mE}, which is metastable eutectic point, salicylamide melts completely and 4-acetamidobenzoic acid melts only partially. The melt components form a cocrystal, which transforms into solid phase. The cocrystal is in equilibrium with the melt (in the area indicated by CC+L of the diagram), and with the melt and excess of solid B (in the area indicated by CC+B+L of the diagram). When heated up to the incongruent melting point T_D or peritectic point - T_P (T_P = 178 °C ≈ T_{CC}), the cocrystal melts, and in the B+L area of the diagram only the melt and the remaining acid coexist until the melting temperature of the component B (point T_F, liquidus line), with the whole mixture transforming into liquid state.

Additional small peaks were observed at 165−168 °C for A:B physical mixtures with the molar rates of 1:10, 1:3, and 2:3 (with an excess of 4-acetamidobenzoic acid). They were marked as red circles in Figure 2. Similar effects were interpreted as cocrystal eutectic melting with an excess of high-melting component in the research done by Yamashita et al.[40] Therefore, we can conclude that the cocrystal 4-acetamidobenzoic acid eutectic fusion occurs within the temperature range of 165−168 °C.

The above presented fusion diagram is well illustrated by the results of hot stage microscopy (Figure 3). The cocrystal melting consists of two stages. At the first stage, the cocrystal melts at 183 °C with decomposition and high-melting 4-acetamidobenzoic acid crystals are formed from the melt. This process corresponds to the CP line (temperature in HSM is slightly higher due to lesser leaktightness of the hot stage).

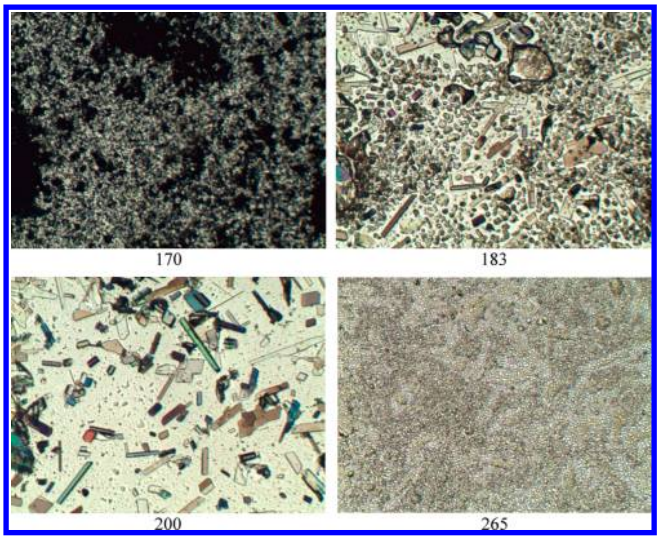

Figure 3. Microscopic observation of thermal behavior of the cocrystal. Polarization microscopic pictures at four temperatures.

Further heating leads to a decrease in the solid fraction of B in the B+L area of the fusion diagram (at 200 °C, see Figure 3). At about 215 °C the high-melting solid phase disappears and at higher temperatures only the liquid remains, as can be seen in Figure 3, 265 °C.

4.2. Ternary Phase Diagram. A ternary phase diagram was plotted in order to find out the optimal conditions for growing cocrystal clear single crystals and preventing the formation of nonstable cocrystal forms. Figure 4 shows a salicylamide-4-

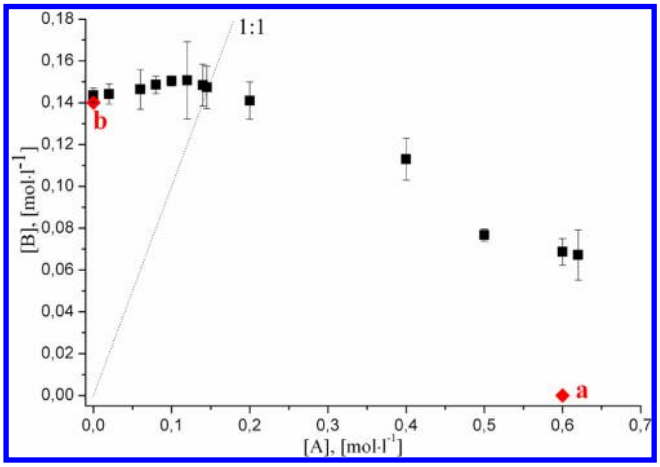

Figure 4. Phase solubility diagram for A-B-EtOH system at 25 °C showing solution concentration of [B] at equilibrium with A (■) in ethanol. Measured solubility of A and B in ethanol are indicated by the points "a" (red diamond) and "b" (red diamond), respectively. Dashed line represents reactant stoichiometry in solution corresponding to that of cocrystal.

acetamidobenzoic acid-ethanol solubility phase diagram. The diagram proves that the 4-acetamidobenzoic acid solubility increases insignificantly if the salicylamide concentration grows, until the 1:1 molar ratio is reached. After the 1:1 molar ratio is reached, the 4-acetamidobenzoic acid solubility in ethanol decreases which indicates higher cocrystal stability in the solvent.

dx.doi.org/10.1021/jp5032898 | J. Phys. Chem. B 2014, 118, 6803−6814

The ternary phase diagram (TPD) is presented in Figure 5. The solubility and stability of different crystalline phases can be estimated by the ternary phase diagram.[9]

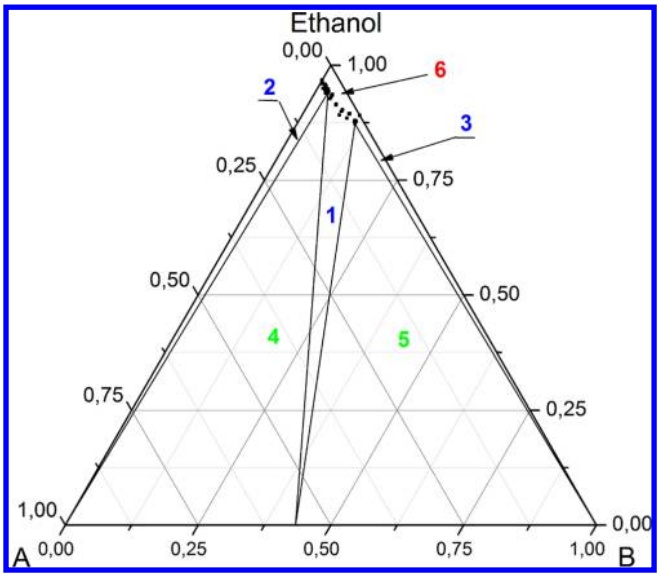

Figure 5. Triangle phase diagram of A-B-EtOH system at 25 °C generated from experimental solubility data. Compositions shown are on mass fraction basis.

The stability domains of the cocrystal, salicylamide and acetamidobenzoic acid solid phases are presented in the triangle diagram as 1, 2, and 3, respectively. Regions 4 and 5 indicate regions where two solid phases are in equilibrium with the solution: A/cocrystal in region 4, B/cocrystal in region 5. The solutions with various compositions are represented by region 6. Therefore, in order to obtain a clear and stable cocrystal, it is necessary to prepare a solution with the same composition as in region 1. Using slow evaporation technique we were able to obtain a single crystal of the cocrystal from ethanol.

4.3. Sublimation Thermodynamic Studies. Despite the active investigation of various physicochemical properties of cocrystals, no papers concerning cocrystal sublimation have been published until now. In our work, the sublimation experiments of the cocrystal were carried out for the first time and thermodynamic properties were determined.

Figure 6 represents temperature dependencies of vapor pressure for cocrystal and its coformers. The temperature dependences of cocrystal components in pure state show that salicylamide saturated vapor pressure at the same experimental temperature (T = 69.85 °C, for example) (Figure 6) is 3 orders of magnitude higher than the analogous value for 4-acetamidobenzoic acid. The sublimation thermodynamic parameters of the individual components are presented in Table 1. Therefore, under the same experimental conditions when salicylamide in the gas phase is in equilibrium with the crystal lattice, the 4-acetamidobenzoic acid is in the supersaturated state. Indeed, the sublimation experiment with the cocrystal has shown that only salicylamide is sublimated. The cocrystal thermogravimetry/mass-spectrometry experiment also indicated that in the vapor phase when the cocrystal temperature is below the melting point, only a low-melting substance (A) is formed with its amount increasing as the temperature rises. (Figure 7). This indicates that at some point

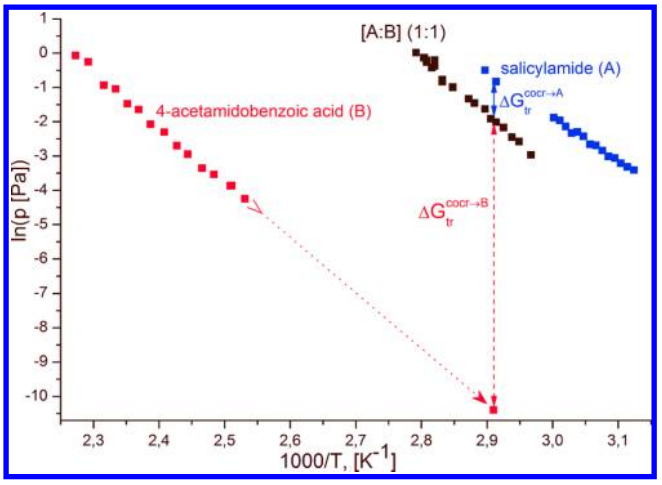

Figure 6. Temperature dependencies of vapor pressure of the cocrystal and its components in pure form.

the cocrystal falls into parts, one of which is volatile and is carried away by the gas flow.

DSC experiments show that the cocrystal in its solid form is thermally stable and does not decompose until T_m = 182.4 °C. Therefore, we can conclude that the cocrystal decomposes in the gas flow but it happens so quickly that only salicylamide molecules get into the mass-spectrometer ionization chamber. However, the amount of the substance carried away is so small that the backward precipitating low-volatile component (B) does not almost change the solid state composition and does not disturb the thermodynamic equilibrium. To prove the equilibrium process, we determined the dependence of the saturated vapor pressure on the temperature and speed of the inert gas-carrier flow (Figure S1). The assumed cocrystal sublimation mechanism is represented in Scheme 2.

The separation of A···B cocrystal molecule from the crystal lattice is accompanied by destruction of all intermolecular interactions. Then, the acid-amide supramolecular heterosynthon breaks down and the cocrystal falls into components among which B crystallizes back to the working surface while salicylamide is carried away by the inert gas-carrier and is sublimated. Therefore, by conducting the sublimation experiment we have obtained the value of the crystal lattice energy, numerically equal to the dissociation energy of all the intermolecular interactions including the cocrystal dimer acid-amide supramolecular heterosynthon.

The thermodynamic parameters of cocrystal sublimation process are presented in Table 2.

It can be noted that the cocrystal has similar vapor pressure value to that of salicylamide but in terms of its crystal lattice energy value it is close to 4-acetamidobenzoic acid. Besides, the entropy term of the cocrystal is substantially higher than that of both components in pure form.

4.4. Crystal Structure Analysis. The results of X-ray single crystal analysis of the cocrystal are presented in Table 3.

It has a 1:1 ratio of salicylamide and acetamidobenzoic acid in the asymmetric unit with Z′ = 2. The two types of heterodimers, denoted as A-B and A′-B′, where A stands for salicylamide and B − 4-acetamidobenzoic acid, forming an asymmetric unit of the cocrystal, are given in Figure 8a,b. According to them, salicylamide molecules have identical conformation state in these heterodimers, whereas acetamidobenzoic acid molecules exist in two different conformation

dx.doi.org/10.1021/jp5032898 | J. Phys. Chem. B 2014, 118, 6803−6814

Table 1. Temperature Dependencies of Vapor Pressure and Thermodynamic Parameters of Sublimation Processes for Cocrystal Components: 2-Hydroxybenzamide (A)[24] and 4-Acetamidobenzoic Acid (B)

A[a]		B[b]	
T [°C]	p [Pa]	T [°C]	p [Pa]
47.0	3.30×10^{-2}	70.0[1]	3.05×10^{-5}
48.0	3.62×10^{-2}	121.9	1.43×10^{-2}
49.0	4.04×10^{-2}	125.1	2.10×10^{-2}
50.0	4.69×10^{-2}	125.4	2.09×10^{-2}
51.0	5.23×10^{-2}	129.4	2.92×10^{-2}
52.0	5.84×10^{-2}	132.4	3.48×10^{-2}
53.0	6.79×10^{-2}	136.0	5.24×10^{-2}
54.0	7.43×10^{-2}	139.0	6.72×10^{-2}
55.0	8.80×10^{-2}	142.2	1.00×10^{-1}
56.0	9.73×10^{-2}	145.8	1.26×10^{-1}
57.0	1.05×10^{-1}	149.0	1.93×10^{-1}
58.0	1.18×10^{-1}	151.9	2.27×10^{-1}
59.0	1.41×10^{-1}	155.4	3.52×10^{-1}
60.0	1.53×10^{-1}	158.6	3.93×10^{-1}
70.0	4.68×10^{-1}	163.1	7.75×10^{-1}
72.0	5.71×10^{-1}	166.9	9.34×10^{-1}
ΔG^{298}_{sub}, [kJ·mol^{-1}]	44.4	ΔG^{298}_{sub}, [kJ·mol^{-1}]	72.3
ΔH^{298}_{sub}, [kJ·mol^{-1}]	106.6 ± 0.7	ΔH^{298}_{sub}, [kJ·mol^{-1}]	138 ± 2
$T\Delta S^{298}_{sub}$, [kJ·mol^{-1}]	62.2 ± 1.5	$T\Delta S^{298}_{sub}$, [kJ·mol^{-1}]	65.7 ± 3
ΔS^{298}_{sub}, [J·mol^{-1}·K^{-1}]	209 ± 4	ΔS^{298}_{sub}, [J·mol^{-1}·K^{-1}]	221 ± 8
T_{fus}, [K]	413.9 ± 0.2	T_{fus}, [K]	535.3 ± 0.2
$\varsigma_{H,}$[c] [%]	63.1	ς_{H},[c] [%]	67.7
$\varsigma_{TS,}$[d] [%]	36.9	ς_{TS},[d] [%]	32.3

[a] $\ln(p(\text{Pa})) = (36.4 \pm 0.3) - (12756 \pm 83)/T$, R = 0.999; $\sigma = 2.09 \cdot 10^{-2}$; $n = 16$. [b] $\ln(p(\text{Pa})) = (36.69 \pm 0.72) - (16198 \pm 299)/T$, R = 0.998; $\sigma = 9.35 \cdot 10^{-2}$; $n = 15$. [c] $\varsigma_H = (\Delta H^{298}_{sub}/(\Delta H^{298}_{sub} + T \cdot \Delta S^{298}_{sub})) \times 100\%$. [d] $\varsigma_{TS} = (T \cdot \Delta S^{298}_{sub}/(\Delta H^{298}_{sub} + T \cdot \Delta S^{298}_{sub})) \times 100\%$.

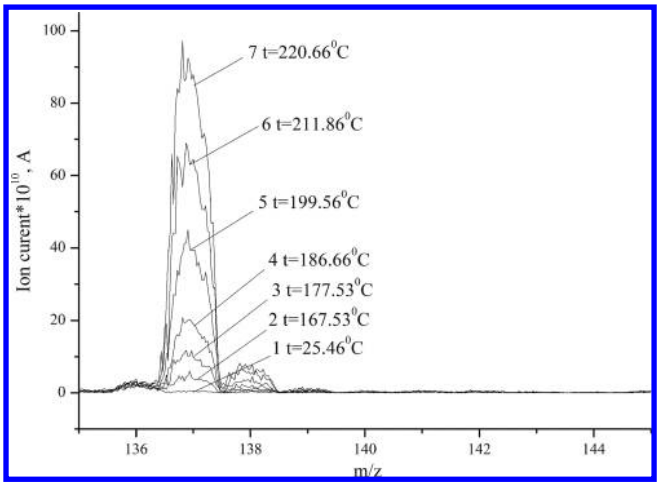

Figure 7. Mass-spectrometric cocrystal vapor composition analysis results.

states. The N2H2 and O3H3 groups are in cis-conformation in the A···B heterodimer, while these groups are in trans-conformation in A′···B′, c.f. Figure 8a,b. The corresponding bond length and bond angles of the B and B′ molecules are close to each other. For example, the difference in the N2C15 and N′2C′15 bond length is around 0.001 Å. Geometrical parameters of intermolecular H-bonds forming by the B and B′ molecules are more sensitive to the conformation state of acetamidobenzoic acid. According to Table 4, the differences between the corresponding N···O distances vary from 0.01 to 0.025 Å.

The heterodimers are stabilized by the acid···amide synthons forming a second level $R^2_2(8)$ motif (Table S2). The O···O and N···O distances are rather short, ∼ 2.60 and ∼2.95 Å, respectively (Table 4). The angle between the planes of the diverse heterodimers is ∼62°, whereas identical heterodimers planes are parallel to each other (Figure 9a). The H−N−C═O group of acetamidobenzoic acid binds the adjacent salicylamide molecules through the two N−H···O bonds to form a ribbon in the *bc*-plane (Figure 9b). The intermolecular N−H···O and O−H···O bonds are generally linear in the range from 164 to 176 deg.

Six molecules of the cocrystal form hexagonal cell ($R^6_6(36)$) by the N−H···O bonds (Figure 9c). The cells are held together by acid-amide synthons and generate infinite zigzag chains. (Figure 9d). These chains are not connected with each other by N−H···O and O−H···O bonds and are held together only by the noncovalent interactions described in subsection 4.5.

4.5. Pattern of Noncovalent Interactions in the Cocrystal. The computed distances between N and O atoms involved in intermolecular H-bonds formation are in reasonable agreement with the experimental data, see Table 5. The N−H···O bonds are characterized by small positive $\nabla^2\rho_b$ values and the electron density ρ_b at the bond critical point lower 0.04 au According to Gatti,[41] these intermolecular H-bonds correspond to the closed-shell interactions. The energy of N−H···O bonds varies from 17 to 27 kJ·mol^{-1}, see Table 5. The strongest N−H···O bond is formed by the N1H1b group of salicylamide and the C′15=O′5 group of the adjacent acetamidobenzoic acid molecule (Figure 11). The intermolecular O−H···O bond is the strongest H-bond in the cocrystal. Its energy is 46 kJ·mol^{-1} (Table 5). This H-bond is characterized by $\rho_b > 0.05$ au and belongs to the intermediate type of interactions.[42]

dx.doi.org/10.1021/jp5032898 | J. Phys. Chem. B 2014, 118, 6803−6814

Scheme 2. Mechanism of Cocrystal Sublimation Process

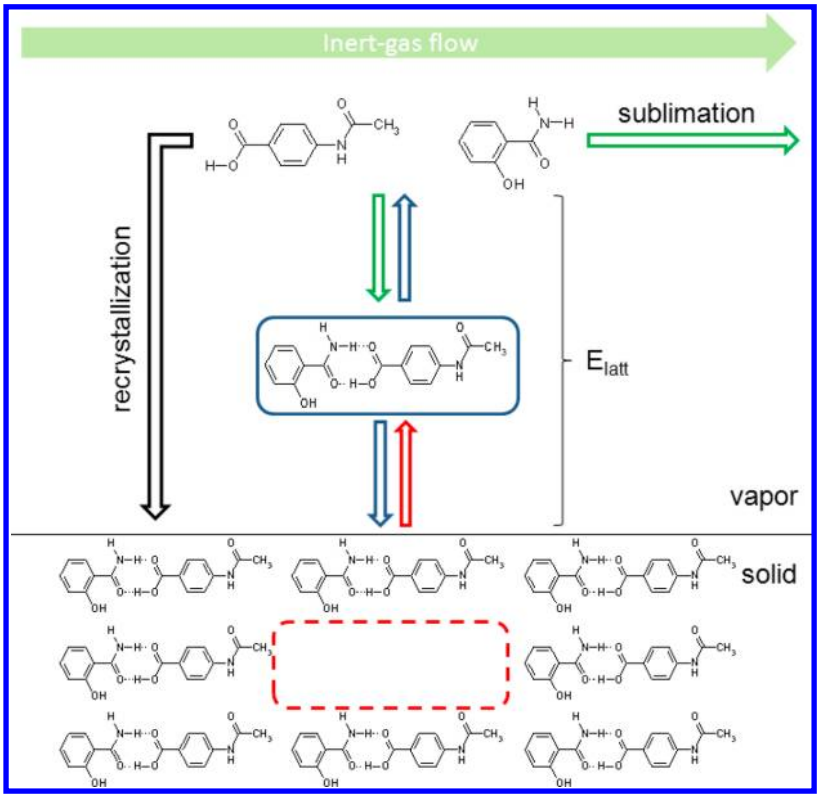

Table 2. Temperature Dependencies of Cocrystal Vapor Pressure and Thermodynamic Parameters of [A:B] (1:1) Cocrystal Sublimation Process[a]

N	T [°C]	p [Pa]	N	T [°C]	p [Pa]
1	63.9	5.14×10^{-2}	9	75.0	2.63×10^{-1}
2	66.0	7.57×10^{-2}	10	78.0	3.69×10^{-1}
3	67.2	8.62×10^{-2}	11	80.0	4.34×10^{-1}
4	68.7	1.14×10^{-1}	12	82.0	6.56×10^{-1}
5	70.0	1.33×10^{-1}	13	83.0	8.08×10^{-1}
6	71.0	1.47×10^{-1}	14	83.5	8.72×10^{-1}
7	72.0	1.96×10^{-1}	15	85.0	1.01
8	74.0	2.33×10^{-1}			
ΔG^{298}_{sub}, [kJ·mol^{-1}]	51.9	$T\Delta S^{298}_{sub}$, [kJ·mol^{-1}]	90.9		
ΔH^{T}_{sub}, [kJ·mol^{-1}]	140 ± 3	ΔS^{298}_{sub}, [J·mol^{-1}·K^{-1}]	305 ± 10		
$\Delta H^{298 b}_{sub}$, [kJ·mol^{-1}]	143 ± 4	T_{fus}, [K]	455.5 ± 0.2		
$C^{298 c}_{p,cr}$, [J·mol^{-1}·K^{-1}]	428.2	$\varsigma_{H,}$ [%][d]	72.3		
		$\varsigma_{TS,}$ [%][e]	27.7		

[a] $\ln(p(\text{Pa})) = (46.93 \pm 1.09) - (16802 \pm 383)/T$, R = 0.99534; $\sigma = 9.12 \times 10^{-2}$; $n = 20$. [b] $\Delta H^{298}_{sub} = \Delta H^{T}_{sub} + [0.75 + 0.15 \cdot C^{298}_{p,cr}(298.15)](T - 298.15)$. [c] Calculated by Chickos's additive scheme.[20] [d] $\varsigma_H = (\Delta H^{0,298}_{sub}/(\Delta H^{0,298}_{sub} + T \cdot \Delta S^{298}_{sub})) \times 100\%$. [e] $\varsigma_{TS} = (T \cdot \Delta S^{0,298}_{sub}/(\Delta H^{0,298}_{sub} + T \cdot \Delta S^{0,298}_{sub})) \times 100\%$.

A lot of atoms of the A-B heterodimer are involved in relatively short contacts with the atoms of the neighbor molecules. However, the existence of short intermolecular contact does not imply the existence of the intermolecular (noncovalent) interaction, e.g. see.[43a] The Bader analysis[34] of the computed periodic electron density enables us to detect and to quantify the noncovalent interactions (besides N−H···O and O−H···O bonds) in the cocrystal. The obtained results are collected in Table 5. According to the QTAIMC analysis, all C−H groups of acetamidobenzoic acid, with the only exception of C16−H16b, are involved in the formation of noncovalent interactions of different types and strength. In contrast to acetamidobenzoic acid, only one group of salicylamide, namely C6−H6, interacts with the adjacent molecule, see Table 5. All oxygen atoms of the salicylamide and acetamidobenzoic acid molecules are involved in the formation of the C−H···O contacts the energies of which vary from ∼5 to 12 kJ·mol^{-1} (Table 5). Such energies are typical of the C−H···O contacts in the gas-phase systems[43] and molecular crystals[33b]. According to the QTAIMC analysis, the salicylamide molecule of the A-B heterodimer interacts with two neighbor acetamidobenzoic acid molecules (Figure 10) through two N−H···O bonds and two C−H···O contacts. The energy of these intermolecular interactions is ∼62 kJ·mol^{-1} (Table 5). The acid-amide heterosynthon and the above-mentioned intermolecular

dx.doi.org/10.1021/jp5032898 | J. Phys. Chem. B 2014, 118, 6803−6814

Table 3. Crystal Lattice Parameters of [A:B] (1:1)

crystal data	cocrystal
CCDC	989 912
formula	$C_{16}H_{16}N_2O_5$
molecular weight	316.31
crystal system	monoclinic
space group	*Pc*
crystal size, mm	0.12 × 0.07 × 0.04
a, Å	10.838(5)
b, Å	11.225(5)
c, Å	13.268(6)
α, °	90
β,°	107.879(7)
γ,°	90
volume, Å^3	1536.3(12)
Z	4
D_{calc}, g·cm^{-3}	1.368
radiation	Mo Kα
T, K	296(2)
μ, mm^{-1}	0.103
Data Collection	
measured reflections	14 141
independent reflections	3349
independent reflections c	2300
$I > 2\sigma(I)$	
R_{int}	0.0875
θ_{max}	27.00
Refinement	
refinement on	F^2
$R[F^2 > 2\sigma(F^2)]$	0.0477
$\omega R(F^2)$	0.1237
S	0.917
reflections	3349
parameters	417
$(\Delta/\sigma)_{max}$	0.000

Table 4. Geometry of the H-Bonded Fragments X-H···O, Where X = N or O of the Cocrystal

interaction[a]	H-bonded fragment[b]	X···H [Å]	H···O [Å]	X···O [Å]	X-H···O [deg]
A···B	N1−H1a···O4	0.860	2.108	2.947	165.3
B···A	O3−H3a···O1	0.820	1.819	2.629	169.6
A···A	O2−H2···O1	0.819	1.773	2.497	146.3
B···A′	N2−H2a···O′2	0.860	2.109	2.967	176.0
B···A′	O5···H1′b-N′1	0.860	2.013	2.854	165.9
A′···B′	N′1-H′1a···O′4	0.860	2.119	2.965	167.8
B′···A′	O′3-H3′a···O′1	0.820	1.799	2.604	167.1
A′···A′	O′2-H′2···O′1	0.820	1.776	2.499	146.2
B′···A	N′2-H′2a···O2	0.860	2.099	2.958	176.5
B′···A	O′5···H1b-N1	0.860	2.034	2.871	163.9

[a]See text and Figures 8 and 10 for definition. [b]See Figure 8 for atomic numeration.

interactions combine together to form a second level $R_6^6(36)$ motif, see Figure 9c.

Different zigzag chains, see Figure 9d, contact each other through weak van-der-Waals interactions (the last two rows in Table 5 and Figures S2, S3). These interactions complete the 3D crystal structure.

According to Scheme 2, the E_{latt} computations in the considered cocrystal may be carried out in two separate steps. First, the acid-amide heterosynthon energy is computed. Then, the interaction energy of the heterodimer with the surrounding molecules is evaluated. Using this approximation, eq 2 may be written in the following way:

$$E_{latt} = (A\cdots B) + [\sum (A\cdots B') + \sum (B\cdots A') + (1/2)\sum (A\cdots A') + (1/2)\sum (B\cdots B')] \quad (4)$$

Here A′ and B′ stand for the molecules interacting with the A-B heterodimer via intermolecular H-bonds, C−H···O contacts, etc. Equation 4 is exact for the two-component crystals with the 1:1 ratio of the A and B components in the

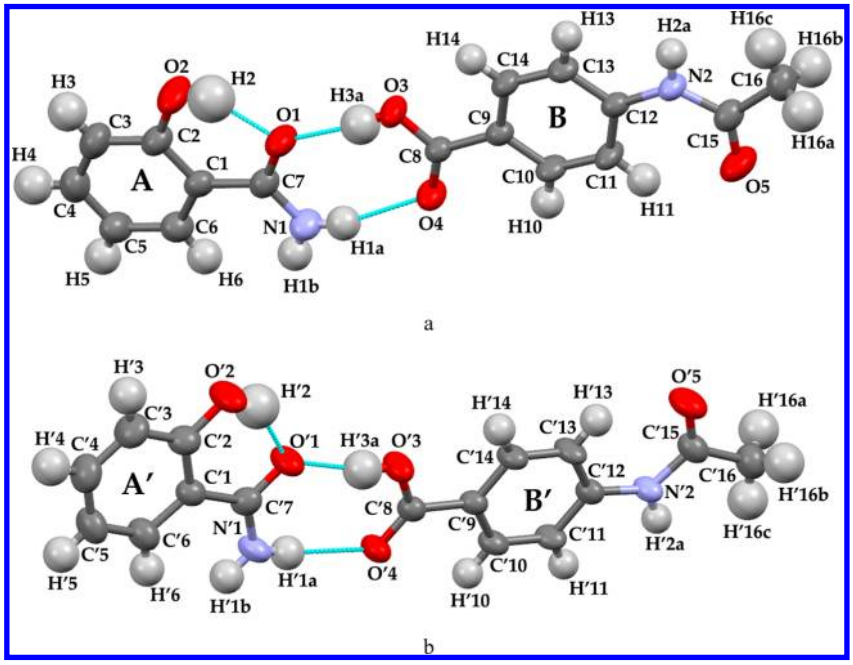

Figure 8. Two types of heterodimers in cocrystal: (a) A···B heterodimer and (b) A′...B′ heterodimer.

dx.doi.org/10.1021/jp5032898 | J. Phys. Chem. B 2014, 118, 6803−6814

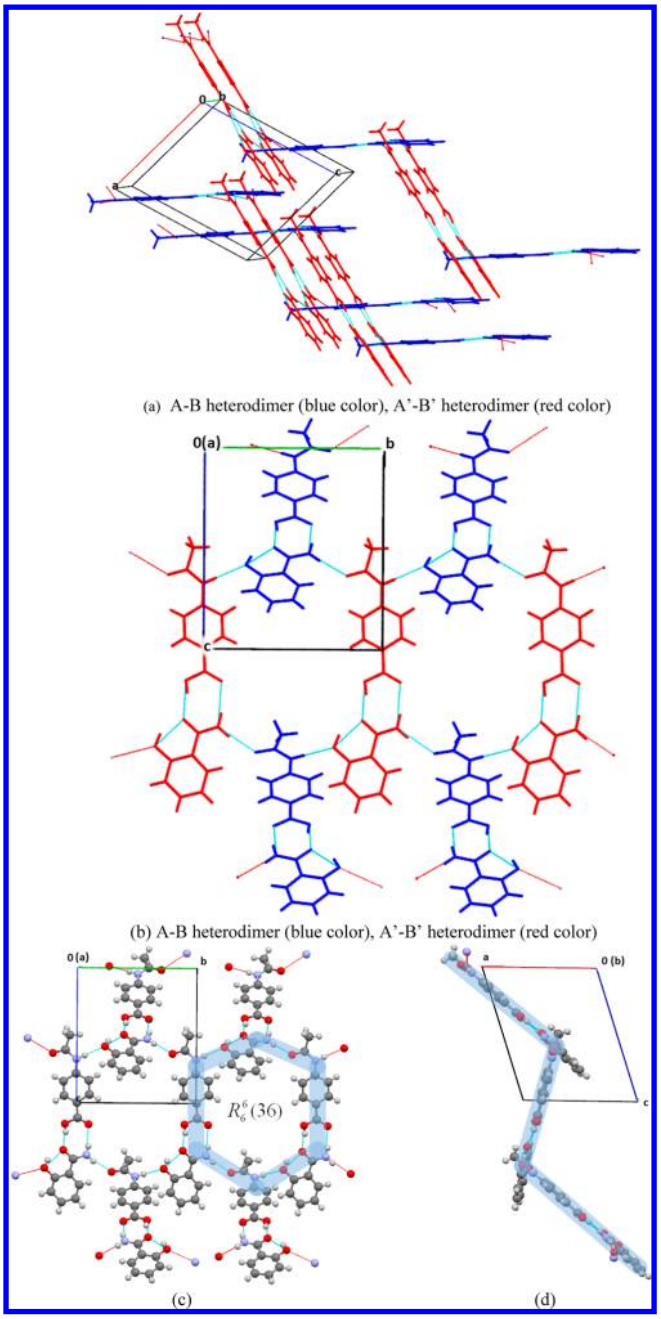

Figure 9. Some features of cocrystal packing.

asymmetric unit and Z′ = 1. The heterosynthon interaction energy is shown by the first term on the right side of eq 4 and denoted as (A···B). The interaction energy of the heterodimer with the surrounding molecules is represented by the second term on the right side of eq 4 and denoted as [...].

The data reported in Table 5 enables one to evaluate the lattice energy of the salicylamide cocrystal using eq 4. The heterosynthon energy equals 68 kJ·mol^{-1}. This value is in good agreement with the energy of 64 kJ·mol^{-1} obtained for the benzamide-salicylic acid cocrystal, see Table 4 in ref 19. The interaction energy of the heterodimer with the surrounding molecules equals 89 kJ·mol^{-1}. According to Table 5, the main contribution to this energy (~62 kJ·mol^{-1}) comes from the interaction of salicylamide with the two neighbor acetamidobenzoic acid molecules, see Figure 10. According to our computations, there is a few kJ·mol^{-1} difference between the E_{latt} values calculated for the A-B and A′-B′ heterodimers. The computed value of the lattice energy of the salicylamide cocrystal equals 156 kJ·mol^{-1}. It is in reasonable agreement with the corresponding energy of 160 kJ·mol^{-1} evaluated for the benzamide-salicylic acid cocrystal.[19]

The calculated lattice energy is assumed to correspond to the sublimation enthalpy ΔH°_{sub}, extrapolated to 0 K. The absolute E_{latt} value is $2RT$ lower than the sublimation enthalpy at the given temperature T.[21] The $2RT$ value at room temperature is less than the error given by the "best" computational methods for the sublimation enthalpy of crystals with moderate H-bonds, see Table S3. That is why the $2RT$ value was omitted in the present study. The value of the lattice energy evaluated using eq 4 equals 156 kJ·mol^{-1}. It agrees with the experimental value 143 ± 4 kJ·mol^{-1}, see Table 2. The experimental value 143 ± 4 kJ·mol^{-1} of the sublimation energy of the salicylamide cocrystal appears to be lower than the sum of the corresponding values of its pure components. This result does not support the thermodynamic argument used in the phenomenological model of Kuleshova et al.[12] According to the latter, the cocrystal can be formed if the absolute value of its total free lattice energy is larger than the sum of the lattice energies of the pure components.

The results of the theoretical study of the noncovalent interactions in the considered cocrystal led to the following conclusions. (1) The acetamidobenzoic acid molecule plays an important crystal-forming role. Its H atoms, with the only exception of one C−H of the methyl group, are involved in the formation of noncovalent interactions of different types and strength. Each oxygen atom of the conformer molecule forms at least one intermolecular O···H−N bond and O···H−C contact. (2) The total energy of the acid-amide heterosynthon and the interaction between salicylamide and the two adjacent acid molecules equals ~130 kJ/mol.

4.6. Solubility Studies. Dissolution measurements of the cocrystal and its components were carried out in phosphate buffer (pH 7.4). The dissolution rate profiles of salicylamide and cocrystal are shown in Figure 11. The equilibrium solubility of cocrystal is 25% higher than that of salicylamide. The DSC analyses of the solid filtrates obtained from the cocrystal dissolution experiment indicate that in buffer (pH 7.4) the [A:B] cocrystal is unstable and breaks down partly into components. A small increase in the salicylamide solubility in the cocrystal in comparison with the pure component can be attributed to the small difference of salicylamide and coformer solubilities in water. As a rule, the API solubility in the cocrystal rises if the coformer solubility more than 10 times exceeds the pure API solubility.[44−46] In case of the compounds under study, the 4-acetamidobenzoic acid solubility is only 2 times higher than the salicylamide solubility in pH 7.4 phosphate buffer.

5. CONCLUSIONS

A novel 1:1 cocrystal of salicylamide and 4-acetamidobenzoic acid was obtained by DSC screening procedure as well as grinding (both neat and solvent-drop) and solvent evaporation techniques. A complete thermal analysis performed by DSC, TG, and hot stage microscopy revealed that the cocrystal remains stable in its solid form until the melting point at 182.4 °C, where it breaks down into components.

To determine the optimal conditions of single crystal growth, a triangle phase diagram for the object system with ethanol was built. An X-ray diffraction experiment with complete solving of the crystal structure was carried out for the cocrystal. The

dx.doi.org/10.1021/jp5032898 | J. Phys. Chem. B 2014, 118, 6803−6814

Table 5. Characteristics of the Intermolecular (Noncovalent) Interactions in the Cocrystal Computed by the Solid-State DFT Method Coupled with the Bader Analysis of the Periodic Wave-Function[a]

interaction[b]	fragment[b]	D(H···Y), Å	D(X···Y)[c], Å	ρ_b, a.u.	E_{int}[d], kJ/mol
A···B	N1H1a···O4	1.915	2.930 (2.965)	0.028	21.9
	O1···H3a-O3	1.604	2.629 (2.604)	0.056	46.2
A···B′	N1H1b···O′5	1.830	2.845 (2.854)	0.032	26.7
	C6−H6···O′5	2.254	3.314 (3.325)	0.014	11.7
	O2···H′2a-N′2	2.035	3.048 (2.967)	0.022	17.1
	O2··· H′16c-C′16	2.561	3.480 (3.478)	0.008	6.9
B···B′	C11−H11···O′4	2.649	3.379 (3.412)	0.007	5.8
	C10−H10···O′4	2.672	3.384 (3.378)	0.006	5.3
	C13−H13···O′3	2.477	3.276 (3.347)	0.009	7.9
B···A′	C14−H14···O′1	3.037	3.740 (3.751)	0.003	2.6
B···A′	C8···C′6		3.419 (3.441)	0.004	3.3
B···B′	H10···H′11	2.496		0.004	2.8
A···B′	H5···C′16	3.001		0.004	2.8
A···B	H4···H16c[e]	2.669		0.003	1.8
B···B	C16−H16a···C14[e]	2.686	3.621 (3.597)	0.009	5.7
B···B	O4···C13[e]		3.664 (3.557)	0.003	2.3

[a]The H···Y distance, D(H···Y), where Y = O, N, C, and H; the electron density ρ_b at the bond critical point; the energy of the intermolecular noncovalent interaction E_{int}. [b]see Figures 8, 9, 10 and Table 4 for definition. [c]D(X···Y) is the distance between X and Y atoms of the X-H···Y fragment, where X = O, N and C. Experimental values are given in parentheses. [d]see Figure S2 for definition. [e]see Figure S3 for definition.

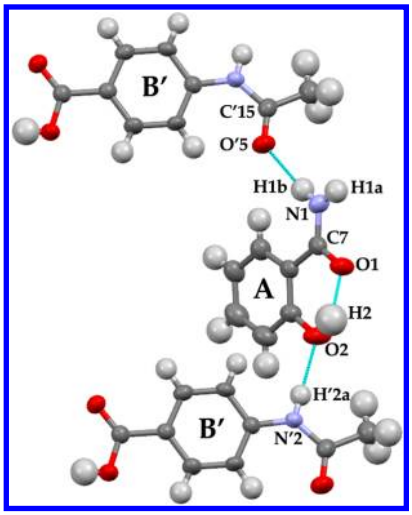

Figure 10. N−H···O intermolecular bond in cocrystal.

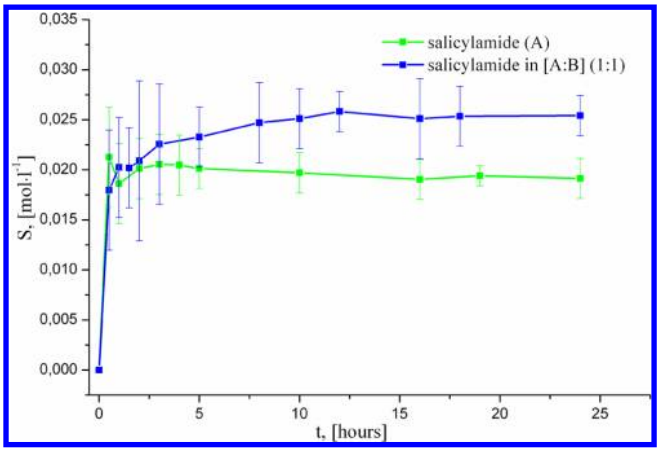

Figure 11. Dissolution rate of salicylamide in cocrystal and in pure form in buffer (pH 7.4).

hydrogen bond network topology analysis coupled with electron density computational modeling in the salicylamide cocrystal has revealed that the molecules are packed in honeycomb-like ribbon structures that are held together by N···O bonds and C···O contacts.

For the first time in literature, the sublimation thermodynamics of a multicomponent crystal was studied experimentally by the transpiration method in a quasi-equilibrium mode. A presumable mechanism of the sublimation process was proposed with the heterodimer sublimating and eventually dissipating into separate molecules. The acetamidobenzoic acid molecules having significantly lower saturated vapor pressure fall back, while more volatile salicylamide is transited with the gas flow into a detecting chamber.

The Bader analysis of the periodic electron density computed using the solid-state DFT methods enables us to quantify the pattern of noncovalent interactions in the salicylamide cocrystal. The main contribution to the interaction of the heterodimer with the surrounding molecules is made by the two N−H···O bonds and the two C−H···O contacts. The total energy of these interactions is around 60 kJ/mol. This result highlights the crystal-forming role of the cocrystal former (acetamidobenzoic acid). 80% of the lattice energy is caused by the acid-amide heterosynthon and the interaction between salicylamide and the two adjacent acid molecules.

Salicylamide in cocrystal shows solubility increase of 25% in 7.4 buffer comparing to the pure form. Such small increase is most likely caused by small difference in water solubilities of components.

■ ASSOCIATED CONTENT

Supporting Information

Details of sublimation experiment and DFT calculations, cocrystal screening results and thorough hydrogen bond network topology analysis. This material is available free of charge via the Internet at http://pubs.acs.org.

dx.doi.org/10.1021/jp5032898 | J. Phys. Chem. B 2014, 118, 6803−6814

AUTHOR INFORMATION

Corresponding Author

*Telephone: +7-4932-533784. Fax: +7-4932- 336237. E-mail glp@isc-ras.ru.

Notes

The authors declare no competing financial interest.

ACKNOWLEDGMENTS

This work was supported by the Federal program for supporting science and innovation (No. 02.740.11.0857), grant of the President of the Russian Federation for young scientists (MK-2309.2013.3), and the Russian Foundation of Basic Research (No. 14-03-01031). DSC experiments were obtained on the equipment of center for joint use of scientific equipment "The upper Volga region center of physico-chemical research".

REFERENCES

(1) Babu, N. J.; Nangia, A. Solubility advantage of amorphous drugs and pharmaceutical cocrystal. *Cryst. Growth Des.* **2011**, *11*, 2662−2679.

(2) Nehm, S. J.; Rodrguez-Spong, B.; Rodrguez-Hornedo, N. Phase solubility diagrams of cocrystals are explained by solubility product and solution complexation. *Cryst. Growth Des.* **2006**, *6*, 592−600.

(3) Karki, S.; Friščic, T.; Jones, W.; Motherwell, W. D. S. Screening for pharmaceutical cocrystal hydrates via neat and liquid-assisted grinding. *Mol. Pharmaceutics* **2007**, *4*, 347−354.

(4) Brittain, H. Pharmaceutical cocrystal: The coming wave of new drug substances. *J. Pharm. Sci.* **2013**, *102*, 311−317.

(5) Good, D. J.; Rodriguez-Hornedo, N. Solubility advantage of pharmaceutical cocrystal. *Cryst. Growth Des.* **2009**, *9*, 2252−2264.

(6) Trask, A. V.; Motherwell, W. D. S.; Jones, W. Physical stability enhancement of theophylline via cocrystallization. *Int. J. Pharm.* **2006**, *320*, 114−123.

(7) Karki, S.; Friščić, T.; Fábián, L.; Laity, P. R.; Day, G. M.; Jones, W. Improving mechanical properties of crystalline solids by cocrystal formation: new compressible forms of paracetamol. *Adv. Mater.* **2009**, *21*, 3905−3909.

(8) Cherukuvada, S.; Babu, N. J.; Nangia, A. J. Nitrofurantoin-p-Aminobenzoic acid cocrystal: Hydration stability and dissolution rate studies. *Pharm. Sci.* **2011**, *100* (8), 3233−3244.

(9) Jayasankar, A.; Reddy, L. S.; Bethune, S. J.; Rodriguez-Hornedo, N. Role of cocrystal and solution chemistry on the formation and stability of cocrystals with different stoichiometry. *Cryst. Growth Des.* **2009**, *9*, 889−897.

(10) Karki, S.; Friščić, T.; Jones, W. Control and interconversion of cocrystal stoichiometry in grinding: stepwise mechanism for the formation of a hydrogen-bonded cocrystal. *CrystEngComm* **2009**, *11*, 470−481.

(11) Issa, N.; Barnett, S. A.; Mohamed, S.; Braun, D. E.; Copley, R. C. B.; Tocher, D. A.; Price, S. L. Screening for cocrystals of succinic acid and 4-aminobenzoic acid. *CrystEngComm* **2012**, *14*, 2454−2464.

(12) Kuleshova, L. N.; Hofmann, D. W. M.; Boese, R. Lattice energy calculation − A quick tool for screening of cocrystals and estimation of relative solubility. Case of flavonoids. *Chem. Phys. Lett.* **2013**, *564*, 26−32.

(13) Fucke, K.; Myz, S. A.; Shakhtshneider, T. P.; Boldyreva, E. V.; Griesser, U. J. How good are the crystallization methods for co-crystals? A comparative study of piroxicam. *New J. Chem.* **2012**, *36*, 1969−1977.

(14) Leyssens, T.; Springuel, G.; Montis, R.; Candon, N.; Veesler, S. Importance of solvent selection for stoichiometrically diverse cocrystal systems: caffeine/maleic acid 1:1 and 2:1 cocrystals. *Cryst. Growth Des.* **2012**, *12*, 1520−1530.

(15) Desiraju, G. R. Crystal Engineering: From Molecule to Crystal. *J. Am. Chem. Soc.* **2013**, *135* (27), 9952−9967.

(16) Steiner, T. The Hydrogen Bond in the Solid State. *Angew. Chem., Int. Ed.* **2002**, *41*, 48−76.

(17) Dunitz, J. D.; Gavezzotti, A. Supramolecular Synthons: Validation and Ranking of Intermolecular Interaction Energies. *Cryst. Growth Des.* **2012**, *12*, 5873−5877.

(18) (a) Reddy, L. S.; Chandran, S. K.; George, S.; Babu, N. J.; Nangia, A. Crystal Structures of *N*-Aryl-*N*′-4-Nitrophenyl Ureas: Molecular Conformation and Weak Interactions Direct the Strong Hydrogen Bond Synthon. *Cryst. Grow. Des.* **2007**, *7*, 2675−2690. (b) Bathori, N. B.; Lemmerer, A.; Venter, G. A.; Bourne, S. A.; Caira, M. R. Pharmaceutical Co-crystals with Isonicotinamide;Vitamin B3, Clofibric Acid, and Diclofenac; and Two Isonicotinamide Hydrates. *Cryst. Growth Des.* **2011**, *11*, 75−87.

(19) Seaton, C. C.; Parkin, A. Making Benzamide Cocrystals with Benzoic Acids: The Influence of Chemical Structure. *Cryst. Growth Des.* **2011**, *11*, 1502−1511.

(20) Chickos, J. S.; Acree, W. E. Enthalpies of Sublimation of Organic and Organometallic Compounds. 1910−2001. *J. Phys. Chem. Ref. Data* **2002**, *31*, 537−698.

(21) Ouvrard, C.; Mitchell, J. B. O. Can we predict lattice energy from molecular structure? *Acta Cryst. B* **2003**, *59*, 676−685.

(22) Brandenburg, J. G.; Alessio, M.; Civalleri, B.; Peintinger, M. F.; Bredow, T.; Grimme, S. Geometrical Correction for the Inter- and Intramolecular Basis Set Superposition Error in Periodic Density Functional Theory Calculations. *J. Phys. Chem. A* **2013**, *117*, 9282−9292 and references therein.

(23) Aakeröy, C. B.; Beatty, A. M.; Helfrich, B. A. A High-Yielding Supramolecular Reaction. *J. Am. Chem. Soc.* **2002**, *124*, 14425.

(24) Manin, A. N.; Voronin, A. P.; Perlovich, G. L. Thermodynamic and structural aspects of hydroxybenzamide molecular crystals study. *Therm. Acta* **2013**, *551*, 57−61.

(25) *CAD-4 Software*, Version 5.0; Enraf-Nonius: Delft, The Netherlands, 1989.

(26) Sheldrick, G. M.; *SHELXL97* and *SHELXS97*. University of Goettingen: Germany, 1997.

(27) Zielenkiewicz, W.; Perlovich, G. L.; Wszelaka-Rylik, M. The vapour pressure and the enthalpy of sublimation. Determination by inert gas flow method. *J. Therm. Analys. Calor.* **1999**, *57*, 225−234.

(28) Dovesi, R.; Saunders, V. R.; Roetti, R.; Orlando, R.; Zicovich-Wilson, C. M.; Pascale, F.; Civalleri, B.; Doll, K.; Harrison, N. M.; Bush, I. J.; et al., *M. CRYSTAL09 (CRYSTAL09 User's Manual)*; University of Torino: Torino, 2009.

(29) Hoser, A. A.; Kamiński, D. M.; Matwijczuk, A.; Niewiadomy, A.; Gagoś, M.; Woźniak, K. On polymorphism of 2-(4-fluorophenylamino)-5-(2,4-dihydroxybenzeno)-1,3,4-thiadiazole (FABT) DMSO solvates. *CrystEngComm* **2013**, *15*, 1978−1988.

(30) Dominiak, P. M.; Espinosa, E.; Angyan, J. In *Modern Charge Density Analysis*; Gatti, C., Macchi, P., Eds.; Springer: London, 2012, 387−433.

(31) (a) Gavezzotti, A. Structure and intermolecular potentials in molecular crystals. *Model. Simul. Mater. Sci. Eng.* **2002**, *10*, R1−R29. (b) Day, G. M. Current approaches to predicting molecular organic crystal structures. *Crystallogr. Rev.* **2011**, *17*, 3−52 and references therein.

(32) Vener, M. V.; Egorova, A. N.; Churakov, A. V.; Tsirelson, V. G. Intermolecular Hydrogen Bond Energies in Crystals Evaluated Using Electron Density Properties: DFT Computations with Periodic Boundary Conditions. *J. Comput. Chem.* **2012**, *33*, 2303−2309.

(33) Saunders, V. R.; Dovesi, R.; Roetti, C.; Causa, M.; Harrison, N. M.; Orlando, R.; Zikovich-Wilson, C. M. *CRYSTAL 98 User's Manual*: Universita di Torino: Torino, 1998.

(34) (a) Bader, R. F. W. *Atoms in Molecules - A Quantum Theory*. Oxford University Press: Oxford, 1990. (b) Tsirelson, V. G. In *The Quantum Theory of Atoms in Molecules: From Solid State to DNA and Drug Design*; Matta, C., Boyd, R., Eds.; Wiley-VCH: Berlin, 2007; Chapter 10.

(35) Gatti, C. *TOPOND98 User's Manual*. CNR-CSRSRC: Milano, Italy, 1999.

(36) (a) Bertini, L.; Cargnoni, F.; Gatti, C. Chemical insight into electron density and wave functions: software developments and applications to crystals, molecular complexes and materials science.

Theor. Chem. Acc. **2007**, *117*, 847−884. (b) Churakov, A. V.; Prikhodchenko, P. V.; Lev, O.; Medvedev, A. G.; Tripol'skaya, T. A.; Vener, M. V. A model proton-transfer system in the condensed phase: NH4+OOH−, a crystal with short intermolecular H-bonds. *J. Chem. Phys.* **2010**, *133*, 164506(9 pages). (c) Vener, M. V.; Medvedev, A. G.; Churakov, A. V.; Prikhodchenko, P. V.; Tripol'skaya, T. A.; Lev, O. H-bond network in amino acid co-crystals with H_2O or H_2O_2. The DFT study of serine-H_2O and serine-H_2O_2. *J. Phys. Chem. A* **2011**, *115*, 13657−13663.

(37) Mata, I.; Alkorta, I.; Espinosa, E.; Molins, E. Relationships between interaction energy, intermolecular distance and electron density properties in hydrogen bonded complexes under external electric fields. *Chem. Phys. Lett.* **2011**, *507*, 185−189.

(38) (a) Shishkina, A. V.; Zhurov, V. V.; Stash, A. I.; Vener, M. V.; Pinkerton, A. A.; Tsirelson, V. G. Noncovalent Interactions in Crystalline Picolinic Acid N-Oxide: Insights from Experimental and Theoretical Charge Density Analysis. *Cryst. Growth Des.* **2013**, *13*, 816−828. (b) Vener, M. V.; Shishkina, A. V.; Rykounov, A. A.; Tsirelson, V. G. Cl···Cl Interactions in Molecular Crystals: Insights from the Theoretical Charge Density Analysis. *J. Phys. Chem. A* **2013**, *117*, 8459−8467.

(39) Lu, E.; Rodriguez-Hornedo, N.; Suryanarayanan, R. A rapid thermal method for cocrystal screening. *CrystEngComm* **2008**, *10*, 665−668.

(40) Yamashita, H.; Hirakura, Y.; Yuda, M.; Teramura, T.; Terada, K. Detection of Cocrystal Formation Based on Binary Phase Diagrams Using Thermal Analysis. *Pharm. Res.* **2013**, *30*, 70−80.

(41) Gatti, C. Chemical bonding in crystals: New directions. *Z. Kristallogr.* **2005**, *220*, 399.

(42) Vener, M. V.; Manaev, A. V.; Egorova, A. N.; Tsirelson, V. G. QTAIM Study of Strong H-Bonds with the O-H···A Fragment (A = O, N) in Three-Dimensional Periodical Crystals. *J. Phys. Chem. A* **2007**, *111*, 1155−1162.

(43) (a) Vener, M. V.; Egorova, A. N.; Fomin, D. P.; Tsirelson, V. G. Hierarchy of the non-covalent interactions in the alanine-based secondary structures. DFT study of the frequency shifts and electron-density features. *J. Phys. Org. Chem.* **2009**, *22*, 177−185. (b) Matta, C. F.; Castillo, N.; Boyd, R. J. Extended Weak Bonding Interactions in DNA: pi-Stacking (Base-Base), Base-Backbone, and Backbone-Backbone Interactions. *J. Phys. Chem. B* **2006**, *110*, 563−528. (c) Scheiner, S. Contributions of NH···O and CH···O Hydrogen Bonds to the Stability of a-Sheets in Proteins. *J. Phys. Chem. B* **2006**, *110*, 18670−18679.

(44) Bolla, G.; Sanphui, P.; Nangia, A. Solubility advantage of tenoxicam phenolic cocrystals compared to salts. *Cryst. Growth Des.* **2013**, *13*, 1988−2003.

(45) Alhalaweh, A.; Roy, L.; Rodriguez-Hornedo, N.; Velaga, S. P. pH-Dependent solubility of Indomethacin-Saccharin and Carbamazepine-Saccharin cocrystals in aqueous media. *Mol. Pharm.* **2012**, *9*, 2605−2612.

(46) Elder, D. P.; Holm, R.; de Diego, H. L. Use of pharmaceutical salts and cocrystals to address the issue of poor solubility. *Int. J. Pharm.* **2013**, *453*, 88−100.